Environmental Pollution 243 (2018) 1057–1067

Contents lists available at ScienceDirect

Environmental Pollution

journal homepage: www.elsevier.com/locate/envpol

Wintertime nitrate formation during haze days in the Guanzhong basin, China: A case study☆

Tian Feng [a, b, c], Naifang Bei [b], Shuyu Zhao [a], Jiarui Wu [a], Xia Li [a], Ting Zhang [a], Junji Cao [a, b], Weijian Zhou [a, c], Guohui Li [a, *]

[a] Key Lab of Aerosol Chemistry and Physics, SKLLQG, Institute of Earth Environment, Chinese Academy of Sciences, Xi'an, China
[b] School of Human Settlements and Civil Engineering, Xi'an Jiaotong University, Xi'an, Shaanxi, China
[c] Xi'an Accelerator Mass Spectrometry Center, Xi'an, China

ARTICLE INFO

Article history:
Received 2 April 2018
Received in revised form
11 September 2018
Accepted 13 September 2018
Available online 18 September 2018

Keywords:
Nitrate
$PM_{2.5}$
HONO
WRF-Chem

ABSTRACT

In this study, the formation of nitrate aerosol from 16 to 24 December 2015 in the Guanzhong basin, China is simulated using the WRF-Chem model. The predicted near-surface O_3, NO_2, and fine particulate matters ($PM_{2.5}$) in the basin and inorganic aerosols and nitrous acid (HONO) in Xi'an are generally in good agreement with the observations. Sensitivity studies show that the heterogeneous HONO sources play an appreciable role in the nitrate formation in the basin, contributing 9.2% of nitrate mass concentrations during heavy haze days. Nitrate formation is also affected by sulfate due to their competition for ammonia, particularly in urban areas. A 50% decrease in SO_2 emissions enhances the nitrate concentration by 6.2% during heavy haze days on average in the basin, and a 50% increase in SO_2 emission reduces the nitrate concentration by 9.7%. The roles of HONO and sulfate competition in nitrate formation are strongly modulated by ammonia. Agricultural emissions predominate the nitrate level in the basin (93.5%), but the non-agricultural sources cannot substantially influence nitrate formation (3.7% −14.6%). Reducing agricultural emission is an effective control strategy to mitigate nitrate pollution in the basin.

1. Introduction

Atmospheric particulate matter (PM) not only exerts important impacts on air quality (Cao et al., 2012b; Feng et al., 2016b; Seinfeld and Pandis, 2006), visibility (Cao et al., 2012b), and human health (Cao et al., 2012c), but also contributes to global and regional climate change (Y. Wang et al., 2014a, 2014b; R. Zhang et al., 2007). Nitrate aerosol, along with sulfate and ammonium, is an important inorganic component of fine particulate matters ($PM_{2.5}$) in the atmosphere (Bian et al., 2017; Karydis et al., 2016; Seinfeld and Pandis, 2006).

Generally, nitrate aerosol is formed through the oxidation of nitrogen oxide ($NO_x = NO + NO_2$) by oxidants such as hydroxyl radical (OH) and ozone (O_3) to produce nitric gas, which then is associated with inorganic cations in the aerosol phase:

$$NO + O_3 \rightarrow NO_2 + O_2 \quad (R1)$$

$$NO_2 + OH + M \rightarrow HNO_3 \leftrightarrow nitrate \quad (R2)$$

$$NO_2 + O_3/O(^3P) \rightarrow NO_3 \quad (R3)$$

$$NO_3 + NO_2 \rightarrow N_2O_5 + H_2O \rightarrow HNO_3 \leftrightarrow nitrate \quad (R4)$$

$$NO_3 + HO_2/HCHO/RCHO/GLY/MGLY\cdots\cdots \rightarrow HNO_3 \leftrightarrow nitrate \quad (R5)$$

In reaction (R5), HCHO is formaldehyde and RCHO is other aldehydes; GLY and MGLY denote glyoxal and methylglyoxal, respectively. The source of NO_x mainly includes anthropogenic emissions from sectors of industry, power plant, and transportation. The nitrate formation is not only determined by the abundance of atmospheric oxidants to convert NO_x to HNO_3 or N_2O_5, but also influenced by sulfate aerosol due to its competition for ammonia in the atmosphere (Lei and Wuebbles, 2013; Morgan

☆ This paper has been recommended for acceptance by Dr. Hageman Kimberly Jill.
* Corresponding author.
E-mail address: ligh@ieecas.cn (G. Li).

https://doi.org/10.1016/j.envpol.2018.09.069
0269-7491/

et al., 2010; Poulain et al., 2011; Seinfeld and Pandis, 2006). Nitrate aerosol is typically formed when sulfate aerosol is neutralized and atmospheric ammonia is in excess. Additionally, HNO_3 can also interact with mineral cations, including calcium, potassium, sodium, and magnesium, and condense into aerosol phase. Previous studies have shown that mineral cations substantially influence nitrate formation in highly polluted areas (e.g., in Mexico City) (Karydis et al., 2011) and on a regional scale (Fairlie et al., 2010; Trump et al., 2015). In addition, the partitioning between gas-phase HNO_3 and nitrate is sensitive to air temperature and relative humidity, i.e., lower temperature is more favorable for nitrate formation (Morgan et al., 2010; Morino et al., 2006; Poulain et al., 2011).

The Guanzhong basin is nestled between the Qinling Mountains and the Loess Plateau, and characterized by a warm and humid climate (Fig. 1). Due to rapid industrialization and urbanization, severe air pollution with exceedingly high levels of $PM_{2.5}$ has frequently engulfed the basin in recent years (e.g. Feng et al., 2016b, 2016a; Shen et al., 2008, 2009), especially during wintertime (Bei et al., 2016a, 2016b; Cao et al., 2012a, 2005). Nitrate aerosol has constituted one of the most important components of $PM_{2.5}$ in the basin, contributing substantially to the haze formation. Shen et al. (2009) have shown that nitrate aerosol contributes more than 25% of water-soluble ions in $PM_{2.5}$ during haze days from October 2006 to September 2007 in Xi'an (the largest city in the basin). Wang et al. (2016) have observed that 13–17% of the non-refractory $PM_{2.5}$ in Xi'an is identified as particle nitrate during the polluted episodes in November ~ December 2012. Therefore, in order to better understand the haze formation and support the design and implementation of emission control strategies, further studies are imperative to investigate the nitrate formation and sources.

The purpose of the present study is to examine the formation of nitrate aerosol in the Guanzhong basin during a 9-day air pollution episode in December 2015 and to verify its main sources using the WRF-Chem model. The WRF-Chem model and its configuration are described in Sect. 2. The model results and discussion are presented in Sect. 3, and the summary is given in Sect. 4.

2. Model and method

2.1. WRF-Chem model

The WRF-Chem model (v3.5.1) (Fast et al., 2006; Grell et al., 2005) with modifications by Li et al. (2011a; 2010; 2011c) from the Molina Center for Energy and the Environment (MCE2) is used to simulate nitrate formation in the Guanzhong basin. This version employs the CMAQ aerosol module developed by US EPA (Binkowski and Roselle, 2003). The inorganic aerosols are predicted using ISORROPIA Version 1.7 (Nenes et al., 1998). Besides the SO_2 gas-phase oxidations by OH and sCI, we adopt a SO_2 heterogeneous reaction parameterization (G. Li et al., 2017). In the parameterization, the SO_2 oxidation in aerosol water by O_2 catalyzed by Fe^{3+} is limited by mass transfer resistances in the gas-phase and gas-particle interface (G. Li et al., 2017). The secondary organic aerosol (SOA) is calculated using a non-traditional SOA module, including the VBS (volatility basis-set) modeling approach and SOA contributions from glyoxal and methylglyoxal (Donahue et al., 2006; Robinson et al., 2007; Tsimpidi et al., 2010). In this module, POA is assumed to be semivolatile and photochemically reactive, and a parameterized approach including nine surrogate species with saturation concentrations from 10^{-2}–$10^{6}\ \mu g\ m^{-3}$ at room temperature is used to represent POA components (Shrivastava et al., 2008). The SOA formation from glyoxal and methlyglyoxal is parameterized as a first-order irreversible uptake by aerosol particles with a reactive uptake coefficient of 3.7×10^{-3} (Volkamer et al., 2007; J. Zhao et al., 2006). The HONO heterogeneous sources are parameterized following Li et al. (2010). In the parameterization, HONO is formed from (1) NO_2 reaction with surface-bound semi-volatile organics (Gutzwiller et al., 2002), (2) NO_2 reaction with freshly emitted soot (Arens et al., 2001), (3) NO_2 reactions on ground surfaces and aerosols (Aumont et al., 2003), and (4) photolysis of HNO_3 adsorbed on the ground surface (Zhou et al., 2003, 2011). The dry deposition of chemical species is parameterized following Wesely (1989) and the wet deposition is according to the method in the CMAQ module. The photolysis rates are calculated using the FTUV module (G. Li et al., 2005; Tie et al., 2003). The aerosol radiative effect is also considered in the version of the WRF-Chem model, based on the New Goddard radiation scheme (Chou and Suarez, 1999), and the aerosol optical depth, single scattering albedo, and asymmetry factor are calculated using the method in Li et al. (2011b). The model is configured with grid spacing of 6 km × 6 km (150 × 150 grid cells) centered at Xi'an (109.0°E, 34.25°N, Fig. 1b). The meteorological boundary and initial conditions are from NCEP 1° × 1° reanalysis data. The chemical boundary and initial conditions are interpolated from Model for OZone And Related chemical Tracers (MOZART) 6 h output (Horowitz et al., 2003). Detailed model configurations are listed in Table 1.

A 9-day episode from 16 to 24 December 2015 is selected for the present study, corresponding to a heavy air pollution event in the Guanzhong basin (Fig. 1a, b, and c). During the period, the observed $PM_{2.5}$ concentration averaged at the monitoring stations in the basin is about $147\ \mu g\ m^{-3}$ and the maximum reaches up to $302\ \mu g\ m^{-3}$. The average temperature and relative humidity at the Jinghe meteorological station (108.97°E, 34.43°N, white dot in Fig. 1b) are 1.5 °C and 56%, respectively, and the average wind speed is around $1.9\ m\ s^{-1}$. It is worth noting that only the washout of air pollutants is calculated in the model, and the entire life cycle of aerosols within clouds and precipitation is still not fully considered. Additionally, there is no precipitation occurrence during the study period in the basin. To better simulate the meteorological fields, surface and upper air observational weather data during the study period are assimilated using four-dimensional data assimilation (FDDA) in the model.

The anthropogenic emissions from Zhang et al. (2009), are employed in the simulation. Fig. 1d and e shows the spatial distributions of NOx and SO_2 emission rates in the study domain, which highlights strong emissions within the Guanzhong basin (circled by dashed lines in the figure). The emissions of various species within the Guanzhong basin in December 2015 are presented in Table S1. Since the Guanzhong basin is next to the vast Loess Plateau in the north, the emission and transport of mineral dust are considered in the model, based on the GOCART dust module (Ginoux et al., 2001). In addition, long-range transport has been reported to be an important factor for local air pollution in Eastern China (Itahashi et al., 2017; Tang et al., 2016; Wu et al., 2018, 2017; Zheng et al., 2015). However, considering that the Guanzhong basin is situated between the Qinling Mountains and the Loess Plateau and only open to the outside in the east, the basin is generally less influenced by the long-range transport (S. Zhao et al., 2015).

2.2. Pollutant measurements

The hourly near-surface NO_2, O_3, and $PM_{2.5}$ mass concentrations released by China's Ministry of Environmental Protection are downloaded from the website http://www.pm25.in. In addition, hourly sulfate, nitrate, and ammonium aerosols in $PM_{2.5}$, and gas-phase HONO at Qujiang Campus, Xi'an Jiaotong University (QJC, XJTU, 109.01°E, 34.23°N, the red dot in Fig. 1b) have been measured during the simulation period using the Gas and Aerosol

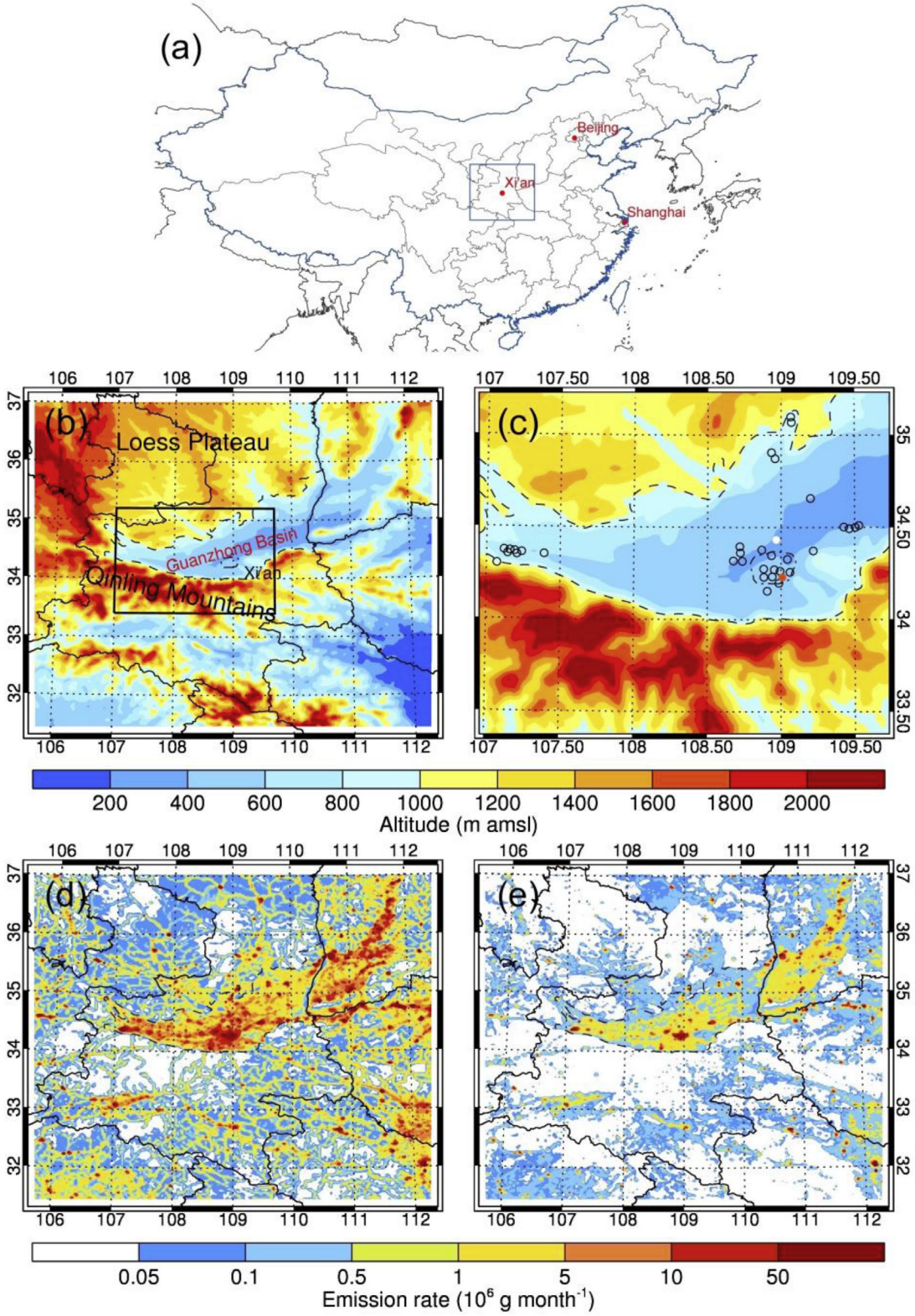

Fig. 1. Map showing (a) the location of the study area in China, (b) the topography of the study area, and (c) geographic distributions of ambient air quality monitoring stations (black circles). The dashed line denotes the boundary of the Guanzhong basin represented by the 1000 m contour and the dash-dotted line shows the area of Xi'an. The white and red dots show the locations of the Jinghe meteorological station and Qujiang Campus, XJTU, respectively. (d) and (e) show the spatial distributions of emission rates of nitrogen oxide (NO_x) and sulfur dioxide (SO_2) in the simulation domain. (For interpretation of the references to color in this figure legend, the reader is referred to the Web version of this article.)

Table 1
Configurations of the WRF-Chem model.

Item	Configuration
Simulation period	December 16–24, 2015
Regions	The Guanzhong basin, China (Fig. 1)
Domain center	Xi'an (109.0°E, 34.25°N)
Domain size	900 km × 900 km
Horizontal resolution	6 km × 6 km
Vertical resolution	35 vertical levels with a stretched vertical grid with spacing ranging from 30 m near surface, to 500 m at 2.5 km and 1 km above 14 km
Microphysics scheme	WRF Single-Moment 6-class scheme (Hong and Lim, 2006)
Boundary layer scheme	MYJ TKE scheme (Janjić, 2002)
Surface layer scheme	MYJ surface scheme (Janjić, 2002)
Land-surface scheme	Noah land surface model (Chen and Dudhia, 2001)
Longwave radiation scheme	New Goddard scheme (Chou et al., 2001)
Shortwave radiation scheme	New Goddard scheme (Chou and Suarez, 1999)
Meteorological boundary and initial conditions	NCEP 1° × 1° reanalysis data
Chemical boundary and initial conditions	MOZART 6-h output (Horowitz et al., 2003)
Anthropogenic emission inventory	SAPRC99 chemical mechanism emissions (Q. Zhang et al., 2009)
Biogenic emission inventory	MEGAN model developed by Guenther et al. (2006)
Model spin-up time	22 h

Compositions Monitor (IGAC, Fortelice International Co., Taiwan) monitoring system. The method detection limits are lower than 0.12 μg m^{-3} (Tian et al., 2017; Young et al., 2016). The instrument background values for most water-soluble inorganic ions are lower than 0.11 μg m^{-3}, except for SO_4^{2-} (1.10 μg m^{-3}) (Tian et al., 2017; Young et al., 2016). Further details on IGAC analysis can be found in Young et al. (2016).

The mean bias (MB), root mean square error (RMSE), and index of agreement (IOA) are used to evaluate the WRF-Chem model simulations against observations.

$$MB = \frac{1}{N}\sum_{i=1}^{N}(P_i - O_i) \quad (1)$$

$$RMSE = \left[\frac{1}{N}\sum_{i=1}^{N}(P_i - O_i)^2\right]^{\frac{1}{2}} \quad (2)$$

$$IOA = 1 - \frac{\sum_{i=1}^{N}(P_i - O_i)^2}{\sum_{i=1}^{N}\left(|P_i - \overline{O}| + |O_i - \overline{O}|\right)^2} \quad (3)$$

where P_i and O_i are the simulated and observed variables, respectively. N is the total number of predictions and $\overline{O}$ denotes the average of observations. IOA has a theoretical range of 0–1, with 1 suggesting perfect agreement between simulations and observations.

3. Results and discussion

3.1. Model performance

For the discussion convenience, we have defined the base simulation in which the emissions from various sources are considered and the heterogeneous HONO formation mechanism is included (G. Li et al., 2010) (hereafter referred to as the REF case), and results from the REF case are compared to observations in the basin.

3.1.1. Simulations of meteorological fields

Considering the crucial role of meteorological conditions in simulating the spatial distribution and temporal evolution of air pollutants (Bei et al., 2016b, 2012), Figure S2 shows the simulated and observed temporal variations of near-surface temperature, relative humidity, wind speed, wind direction, and boundary layer height at the Jinghe meteorological station (Fig. 1c). Note that the boundary layer height estimates are obtained from European Center for Medium-Range Weather Forecasts (ECMWF) reanalysis. The model fairly well reproduces the observed diurnal cycles of temperature and relative humidity, varying from −7 °C to 10 °C and from 20% to 90%, respectively. In general, the observed low wind speeds (<5 m s^{-1}) accompanied by changing wind directions during the haze episode are reasonably simulated, although overestimations occur occasionally. Figure S1e shows that the ECMWF boundary layer height varies dramatically, reaching over 1000 m during daytime and decreasing to less than 100 m during nighttime. The model reasonably replicates the ECMWF boundary layer height, but biases still exist, especially during the daytime from 21 to 24 December 2015.

3.1.2. Simulations of $PM_{2.5}$, O_3, and NO_2

The simulated and observed temporal profile of $PM_{2.5}$ concentrations averaged over the monitoring sites in the basin is shown in Fig. 2a. The observed $PM_{2.5}$ temporal variation distinctly shows a severe haze pollution episode occurred in the basin, including four stages: (1) startup with the slow growth of $PM_{2.5}$ concentrations during 00:00 16–16:00 17 December (local time, hereafter); (2) development with rapid accumulation of $PM_{2.5}$ concentrations during 17:00 17–08:00 21 December; (3) maturation with the $PM_{2.5}$ concentration fluctuation between 200 and 300 μg m^{-3} during 09:00 21–04:00 24 December; and (4) dissipation with very fast falloff of $PM_{2.5}$ concentrations during 05:00–16:00 24 December 2015. The model generally reproduces the haze startup, development, maturation, and dissipation stages, with an *IOA* of 0.92 for the simulated $PM_{2.5}$ concentration. The model slightly underestimates the $PM_{2.5}$ concentration, with a *MB* of −8.9 μg m^{-3}, and the *RMSE* is rather large, showing considerable dispersions of the $PM_{2.5}$ simulation. It is worth noting that $PM_{2.5}$ concentrations are considerably underestimated during the maturation stage. Organic aerosols (OA) are one of the most important components of $PM_{2.5}$, constituting around 30% of $PM_{2.5}$ mass in the basin (Huang et al., 2014). During the maturation stage, the simulated OA mass concentration only contributes about 20% of the observed $PM_{2.5}$ concentration averaged at monitoring sites. Therefore, underestimation of OA concentrations might be one of the possible reasons

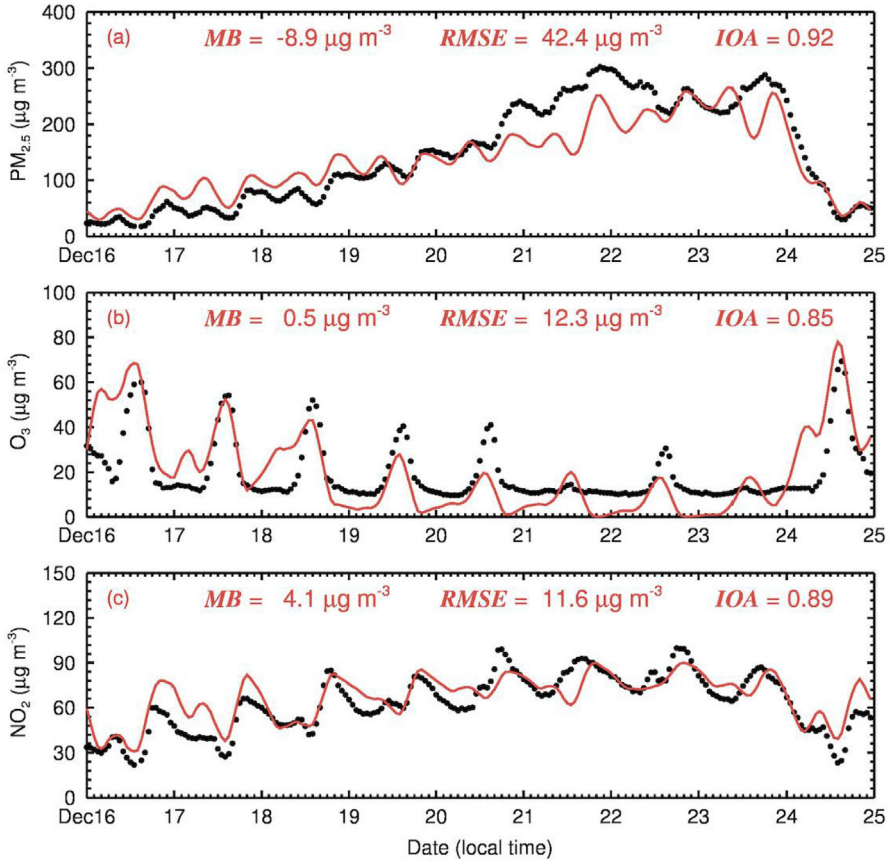

Fig. 2. Diurnal variations of the simulated (red curves) and observed (black spots) (a) $PM_{2.5}$, (b) O_3, and (c) NO_2 concentrations in the Guanzhong basin. Data are averaged over the ambient air quality monitoring stations in the basin. (For interpretation of the references to color in this figure legend, the reader is referred to the Web version of this article.)

for the bias of the $PM_{2.5}$ simulation. In addition, long-range transport has been reported to be an important factor for local air pollution in Eastern China (Itahashi et al., 2017; Tang et al., 2016; Wu et al., 2018, 2017; Zheng et al., 2015). However, considering the situation of the Guanzhong basin as discussed in Section 2.1, the basin is generally less influenced by the long-range transport (S. Zhao et al., 2015). The model also performs reasonably in simulating temporal variations of O_3 and NO_2 concentrations against observations in the basin, with *IOA*s of 0.85 and 0.89, but considerably underestimates the O_3 minimums during the haze nights, which is perhaps caused by the setting of the lower detection limit for O_3 observations.

Fig. 3 shows the distributions of predicted and observed near-surface $PM_{2.5}$ mass concentrations averaged during the startup, development, and maturation stages in the basin. Generally, the predicted $PM_{2.5}$ spatial evolution is consistent with the observations at monitoring sites in the basin. The observed and simulated $PM_{2.5}$ concentrations increase from about 35 to 75 $\mu g\,m^{-3}$ during the startup stage to 150–400 $\mu g\,m^{-3}$ during the maturation stage, indicating the air quality deteriorated from good to severely polluted condition in the basin (Feng et al., 2016a). It is worth noting that the model considerably overestimates the $PM_{2.5}$ concentrations in the central basin against observations during the startup period (Figs. 2a and 3a). One of the most possible reasons for overestimation is the uncertainty of simulated meteorological fields, which determine the formation, transformation, diffusion, transport, and removal of the air pollutants in the atmosphere (Bei et al., 2017). In addition, Figure S2 shows the simulated $PM_{2.5}$ and PM_{10} concentrations due to mineral dust in the study domain, indicating that the $PM_{2.5}$ concentration from dust is rather low in the basin.

3.1.3. Simulations of sulfate, nitrate, and ammonium aerosols, and HONO

Fig. 4 presents the temporal profiles of simulated and measured mass concentrations of sulfate, nitrate, and ammonium aerosols, and HONO at the QJC site in Xi'an from 16 to 24 January 2016. The temporal variations of simulated inorganic aerosols are generally consistent with the measurements, with *IOAs* of 0.89–0.96 (Fig. 4a–c). The simulated and observed sulfate concentrations increase from less than 10 to around 90 $\mu g\,m^{-3}$ from the startup to maturation stage. The model frequently underestimates sulfate concentration with a MB of $-8.6\,\mu g\,m^{-3}$, especially during the maturation stage. Besides SO_2 emissions and simulated meteorological fields, SO_2 oxidation mechanism also plays a key role in the sulfate simulation. Zheng et al. (2015) have proposed that the production rate of sulfate through heterogeneous chemistry can explain the high sulfate concentration during haze episodes. Recent studies have also proposed that the oxidation of SO_2 by NO_2 on neutral aerosols could interpret the efficient sulfate formation during wintertime haze events (Cheng et al., 2016; L. Li et al., 2018; G. Wang et al., 2016), but this pathway for sulfate formation is still controversial. Studies have reported that ambient fine mode aerosols are consistently, and often strongly, acidic (Guo et al., 2017, 2016; 2015). In northern China, fine particles are moderately acidic with a pH ranging from 3.0 to 4.9 (Liu et al., 2017). These mechanisms are not considered in the simulation, which might constitute a main reason for underestimation of sulfate aerosols in the study.

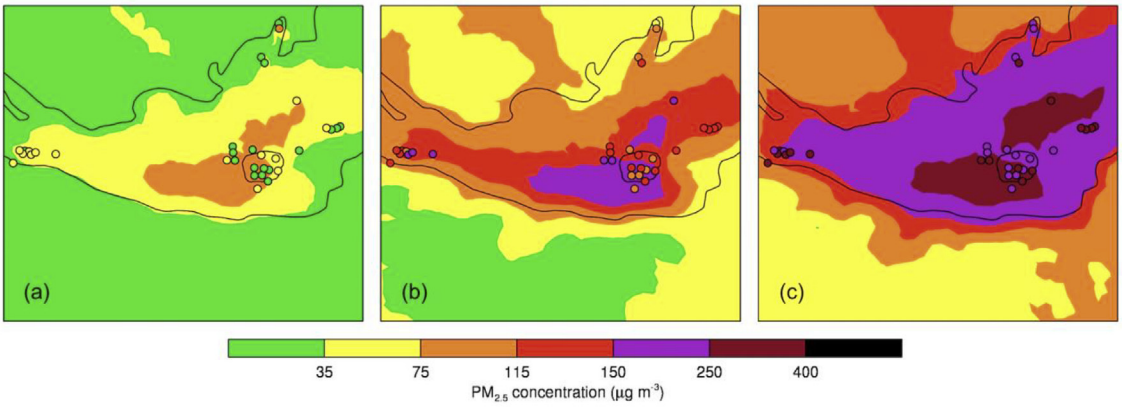

Fig. 3. Spatial distributions of the simulated (colored shadings) and observed (colored spots) $PM_{2.5}$ concentrations averaged over the (a) startup, (b) development, and (c) maturation episodes in the Guanzhong basin. Levels are $PM_{2.5}$ concentration limits in air quality standards of China MEP.

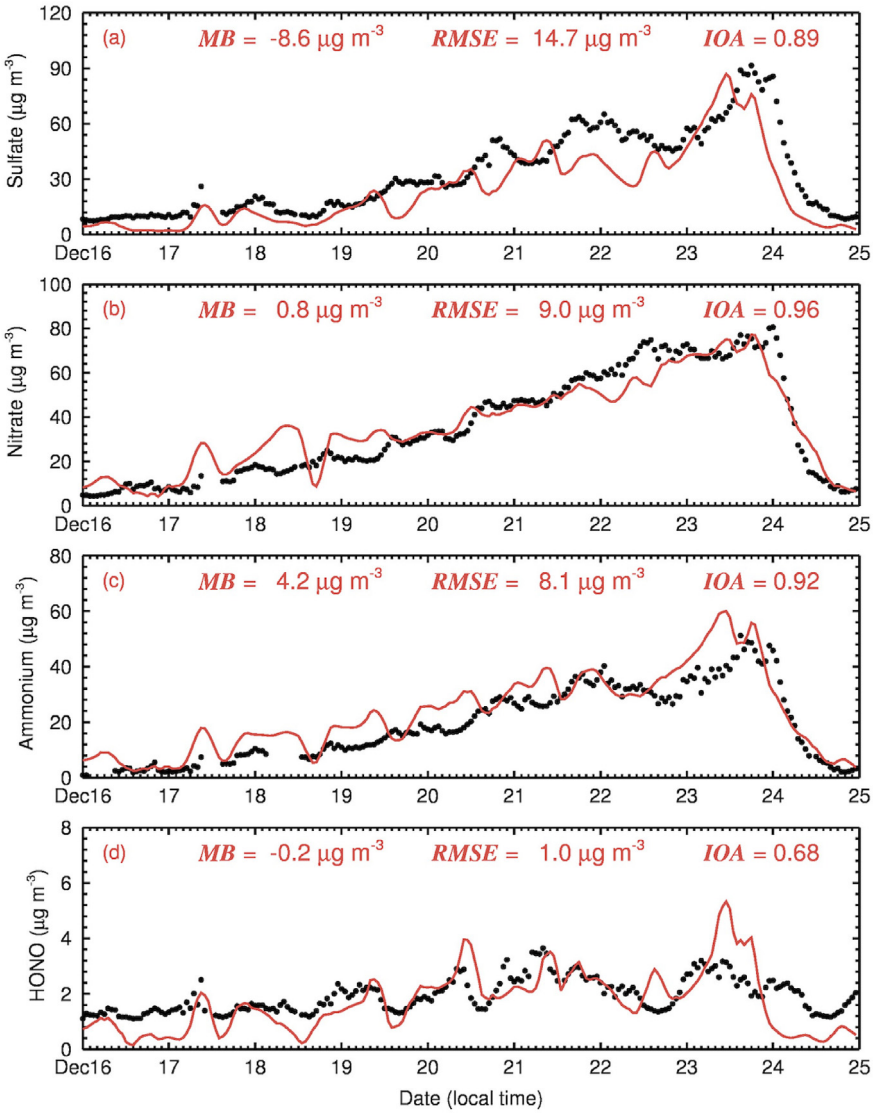

Fig. 4. Diurnal variations of the simulated (red curves) and observed (black spots) (a) sulfate, (b) nitrate, and (c) ammonium aerosols, and (d) gas-phase HONO concentrations at the QJC site. (For interpretation of the references to color in this figure legend, the reader is referred to the Web version of this article.)

Further studies need to be conducted to include the sulfate formation mechanism in the WRF-Chem model to improve the sulfate simulation, associated with possible observed aerosol pH. The simulated sulfate concentration also exhibits large fluctuations, with a *RMSE* of 14.7 $\mu g\ m^{-3}$. On 23 and 24 December, there is a shift between the predicted and observed sulfate aerosols in Fig. 4a. During recent years, the SO_2 emission has been substantially mitigated in Xi'an, so the sulfate aerosol in Xi'an is mainly contributed by the transport from outside of Xi'an. Uncertainties in the simulated wind field, such as biases in the wind speed or direction, can potentially contribute to differences between predicted and observed trace gases and aerosols. During the maturation stage, the observed nitrate concentration fluctuates between 60 and 80 $\mu g\ m^{-3}$, close to the sulfate concentration, showing that the nitrate aerosol has become an important contributor of the heavy haze formation. It is worth noting that the NO_2 concentration is generally well reproduced during the maturation period (Fig. 2c), but the nitrate aerosol is underestimated. There are two main possible reasons for the nitrate underestimation. Firstly, this bias is probably caused by the underestimation of oxidants in the atmosphere, e.g., O_3 concentration (Fig. 2b). Secondly, nitrate concentration can be substantially influenced by the presence of mineral cations (Karydis et al., 2016). Long range transport of dust from the north (Gobi desert) or the west (Taklimakan desert) has provided high levels of background mineral cations in the basin (Huang et al., 2014). However, this modified version of the WRF-Chem model is still lack of treatment of mineral dust thermodynamics, causing the underestimation of nitrate aerosols. The temporal variation of ammonium is also well predicted compared to measurements, with a *MB* of 4.2 $\mu g\ m^{-3}$ and a *RMSE* of 8.1 $\mu g\ m^{-3}$. During the maturation period, the trend of nitrate aerosols shows a plateau, quite different from sulfate and ammonium aerosols. Considering that SO_2, as the precursor of sulfate aerosols, is mainly emitted from point sources, such as power plants or agglomerated industrial zones, the transport of SO_2 from point sources to the observation site is more sensitive to the wind field simulation uncertainties, causing large fluctuations of simulated sulfate aerosols and further ammonium aerosols. The relatively high HONO concentrations are observed during the episode, ranging from 1 to 4 $\mu g\ m^{-3}$ (about 0.5–2 ppb) (Fig. 4d). A recent study has reported that the measured HONO level is about 0.02–4.3 ppb, with an average of 1.12 ppb from 24 July to 6 August 2015 in Xi'an (Huang et al., 2017). The model tracks the observed temporal variation of the HONO concentration at the QJC site, with an *IOA* of 0.68, but model bias is still rather large.

It is worth noting that the simulated temporal variations of inorganic aerosols and HONO concentrations frequently exhibit rather large fluctuations against measurements at the QJC site. One of the most possible reasons is that the QJC site is located at the periphery of Xi'an. The uncertainties in simulated wind fields substantially influence the transport of the pollution plume formed in the urban area of Xi'an, causing the large variability of simulated inorganic aerosols and HONO concentrations (Bei et al., 2017).

3.2. Sensitivity studies

3.2.1. Role of HONO

HONO becomes a key precursor of the hydroxyl radical when the O_3 level is low in the atmosphere (G. Li et al., 2010). During wintertime, fairly low O_3 concentrations have been observed in the Guanzhong basin, particularly during heavy haze episodes (G. Li et al., 2017). Hence, a sensitivity study is performed to verify contributions of the heterogeneous HONO source to the nitrate formation in the basin, in which the heterogeneous HONO source is excluded in the simulation (hereafter referred to as HONO#0). Fig. 5 presents the spatial distributions of the change of average nitrate and $PM_{2.5}$ mass concentrations during the maturation episode (defined as (HONO#0 – REF)). In most areas of the basin, the heterogeneous HONO source contributes at least 6 $\mu g\ m^{-3}$ of the nitrate and more than 15 $\mu g\ m^{-3}$ of the $PM_{2.5}$ concentrations. On average, when the heterogeneous HONO source is not considered in simulations, the nitrate and $PM_{2.5}$ concentrations are decreased by 9.2% (4.6 $\mu g\ m^{-3}$) and 8.3% (15.1 $\mu g\ m^{-3}$) during the maturation episode in the basin, respectively, showing that the HONO source plays an appreciable role in the nitrate and $PM_{2.5}$ formation during the haze pollution. Previous studies have shown that heterogeneous HONO sources enhance secondary aerosol formation, such as SOA and nitrate, and further $PM_{2.5}$ concentrations in Mexico City (G. Li et al., 2010) and North China Plain (An et al., 2012; Y. Li et al., 2011). It is worth noting that the contribution of the heterogeneous HONO source to nitrate and $PM_{2.5}$ is apparently less in urban Xi'an, which is mainly due to the deficiency of ammonia (NH_3) therein.

3.2.2. Impacts of sulfate competition

Since September 2013, stringent control strategies have been implemented in China to mitigate pollutant emissions, particularly with regard to SO_2, and previous studies have shown substantial decrease of SO_2 concentrations in China in recent three years (G. Li et al., 2017). Considering sulfate competition with nitrate for ammonium in the atmosphere (Lei and Wuebbles, 2013; Seinfeld and Pandis, 2006), the decrease or increase of the sulfate formation potentially affects the nitrate level. Therefore, two sensitivity studies are devised, in which the sulfate precursor, SO_2 emission is increased and decreased by 50% in simulations (hereafter referred to as SO_2#1.5 and SO_2#0.5), respectively.

Fig. 6 shows the spatial distributions of the change of average nitrate and $PM_{2.5}$ mass concentrations when the SO_2 emission is increased and decreased by 50% during the maturation episode (defined as (SO_2#1.5 – REF) and (SO_2#0.5 – REF), respectively). When the SO_2 emission is decreased by 50%, indicating less sulfate formation to compete with nitrate for ammonia, the nitrate concentration is enhanced by 2–4 $\mu g\ m^{-3}$ in the east part of the basin and almost 0 in the west part. The most remarkable enhancement occurs in the urban areas of Xi'an (up to 10 $\mu g\ m^{-3}$). Such results imply that there is sufficient ammonia in the west part of the basin and less in the east part, which have potentials to, in part, balance both sulfate and nitrate aerosols under the current emission situation. But ammonia competition exists in Xi'an and sulfate and nitrate concentrations are fairly high, indicative of insufficient ammonia. The deduced spatial pattern of ammonia is accordant with the distribution of farmland which serves as the most important ammonia source in the basin. As expected, when the SO_2 emission is increased by 50%, the spatial decrease of nitrate is similar, i.e., almost 0 in the west part of the basin, higher in the east part, and remarkable in Xi'an. Overall, when the SO_2 emission is decreased or increased by 50%, on average during the maturation episode in the basin, the nitrate concentration is enhanced by 6.2% or reduced by 9.7%, and the $PM_{2.5}$ concentrations are reduced by 4.7% or enhanced by 3.2%, indicating that mitigation of SO_2 emissions is still an effective strategy to improve the local air quality.

3.2.3. Contributions of various anthropogenic sources

Five sensitivity studies are conducted to explore the nitrate contribution of various anthropogenic sources, in which the agricultural, industry, power plant, residential living, or transportation source is excluded individually (hereafter referred to as AGR#0, IND#0, POW#0, RES#0, and TRA#0). An additional sensitivity study with half anthropogenic emissions is also performed to investigate the overall effect of the emission reduction on the nitrate formation (hereafter referred to as ANT#0.5).

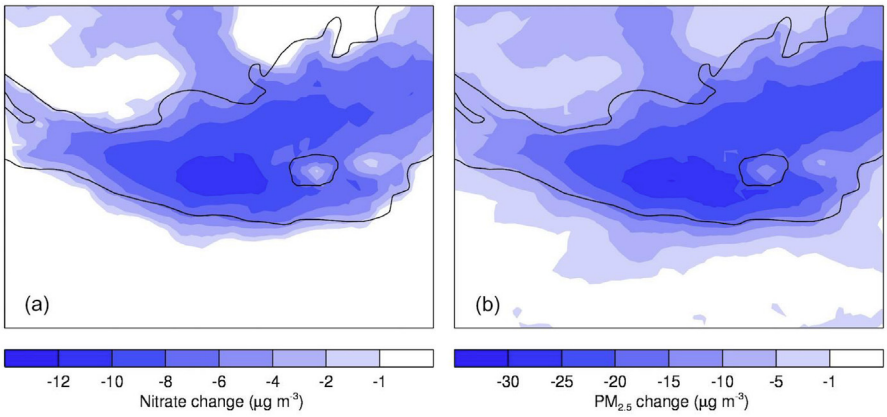

Fig. 5. Spatial patterns of nitrate and $PM_{2.5}$ concentration change averaged over the maturation episode with the heterogeneous HONO sources excluded.

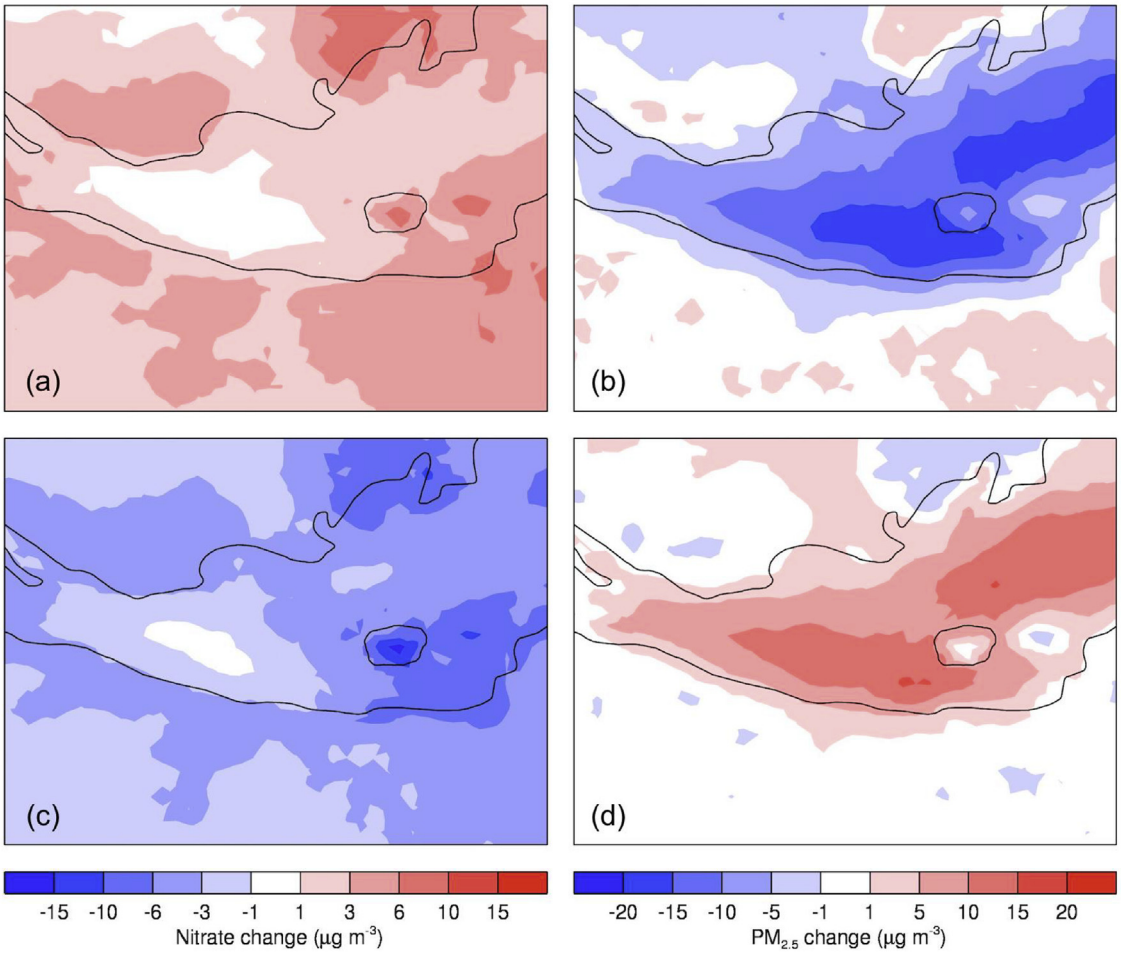

Fig. 6. Spatial patterns of nitrate and $PM_{2.5}$ concentration changes averaged over the maturation episode when SO_2 emissions are changed by ±50%. The top and bottom panels show −50% and +50% alterations, respectively.

Fig. 7 presents the average mass concentration changes in the sensitivity studies compared to the REF case during the maturation period in the basin. Agricultural emission (NH_3) plays an essential role in nitrate formation in the basin, as suggested by previous studies (Pozzer et al., 2017); when the agricultural emission is not included in the model, the nitrate concentration is reduced by 93.5% (46.8 μg m^{-3}), and the $PM_{2.5}$ concentration is also decreased by 43.9% (80.4 μg m^{-3}). The residential source constitutes the second most important nitrate contributor, accounting for about 14.6% of nitrate concentrations in the basin, followed by industry (8.5%), transportation (6.2%), and power plant (3.7%) source. Hence, reducing agricultural emission is the key for the mitigation of nitrate aerosol pollution in the basin. When the total anthropogenic emissions are decreased by 50%, the average nitrate level in Xi'an is

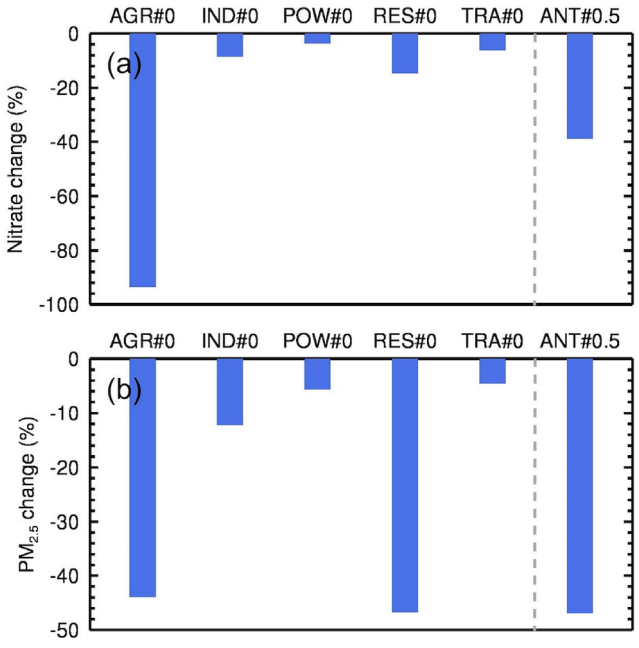

Fig. 7. Percentage changes of (a) nitrate and (b) $PM_{2.5}$ concentrations in the basin during the maturation episode in the sensitivity experiments in different anthropogenic emission scenarios.

reduced by 38.9%. Nitrate formation is complicated, depending on the atmospheric oxidation capability (AOC) and the concentrations of NO_2, sulfate, and ammonia in the atmosphere. Excluding one of the five sources decreases the level of NO_x, volatile organic compounds (VOCs), and SO_2. Decrease of VOCs concentrations generally lowers O_3 production in Xi'an (Feng et al., 2016b), but during wintertime, NO_x decrease is apt to increase O_3 concentration due to the weakened titration effect when the O_3 photochemical production is slow caused by fairly weak insolation, particularly during haze days (Table 2). Although the HONO concentration is lowered due to NO_2 decrease, the O_3 increase compensates the AOC loss due to the HONO decrease or even enhance the AOC. Additionally, decrease of SO_2 emissions also reduce the sulfate formation to make more ammonia available, facilitating the nitrate formation. The complex formation process of nitrate aerosol poses a dilemma for the mitigation of nitrate pollution when reducing non-agricultural emissions.

Fig. 7b shows that the agricultural and residential emissions dominate the haze pollution in the basin, and exclusion of the sources decrease the $PM_{2.5}$ concentration by about 43.9% and 46.7%, respectively. The industry source contributes about 12.2% of the average $PM_{2.5}$ concentration, but the average $PM_{2.5}$ contribution of the power plant and transportation source is not significant, making up 5.6% and 4.5% of the average $PM_{2.5}$ concentration, respectively. Hence, stringent control strategies should be implemented to mitigate emissions from the agricultural and residential emissions to improve the air quality in the Guanzhong basin.

Table 2
The levels ($\mu g\ m^{-3}$) and percentage changes (%, in the bracket) of key species during the maturation episode in the base run and sensitivity experiments.

Case	O_3	HONO	NO_2	NH_3	Sulfate
REF	32.1	1.0	49.4	9.4	15.1
AGR#0	32.8 (2.2)	1.0 (−0.2)	49.0 (−0.8)	0.4 (−96.1)	11.3 (−24.7)
IND#0	38.9 (21.3)	0.8 (−21.3)	38.9 (−21.4)	10.9 (16.4)	11.6 (−23.2)
POW#0	48.0 (49.8)	0.7 (−30.4)	33.4 (−32.5)	11.6 (23.8)	10.4 (−31.0)
RES#0	32.8 (2.2)	0.7 (−30.5)	42.6 (−13.8)	10.5 (11.6)	9.7 (−35.8)
TRA#0	39.8 (24.1)	0.7 (−32.7)	39.7 (−19.6)	9.8 (4.8)	15.1 (0.2)
ANT#0.5	49.8 (55.3)	0.5 (−54.5)	26.9 (−45.6)	3.8 (−59.1)	7.4 (−50.8)

4. Summary and conclusions

In this study, a 9-day episode from 16 to 24 December 2015 corresponding to a severe haze pollution episode is simulated using the WRF-Chem model to investigate the wintertime nitrate formation in the Guanzhong basin, China. Surface and upper air observational weather data during the study period are assimilated using the FDDA method to better simulate meteorological fields.

Generally, the version of the WRF-Chem model used in this study performs reasonably well in simulating the temporal variations of $PM_{2.5}$, O_3, and NO_2 mass concentrations and the $PM_{2.5}$ spatial distributions compared to observations at the monitoring sites. The temporal variations of inorganic aerosols and HONO concentrations are also reasonably reproduced against the measurements by the IGAC system at the QJC site.

Sensitivity studies show that the heterogeneous HONO source plays an appreciable role in the nitrate formation in the Guanzhong basin, with a contribution of 9.2% ($4.6\ \mu g\ m^{-3}$) on average during the severely polluted episode. The sulfate formation also influences the nitrate level due to competition for the ammonia in the atmosphere. With a 50% decrease or increase in the SO_2 emission, the average nitrate concentration in the basin is increased by 6.2% or decreased by 9.7%. The roles of HONO and sulfate competition in nitrate formation are both strongly modulated by the abundance of ammonia in the basin. Among the anthropogenic sources, agricultural emission predominates the nitrate formation in the basin, but none of the rest 4 sources significantly affect nitrate formation due to its complicated formation process. Model results suggests that reducing agricultural emissions is an efficient control strategy to alleviate nitrate pollution in the basin, but mitigation of the non-agricultural sources cannot substantially decrease nitrate formation.

Although the WRF-Chem model reasonably captures the temporal variations or spatial distributions of air pollutants, inorganic aerosol species and HONO compared to observations in the basin, the model biases still exit, particularly for the HONO simulation. Future studies need to be conducted to improve the WRF-Chem model simulations, considering the rapid changes in anthropogenic emissions since the implementation of the Air Pollution Prevention and Control Action Plan in 2013 and uncertainties in the meteorological fields simulations. The oxidation of SO_2 by NO_2 on neutral aerosols and impacts of mineral cations on nitrate formation should be included in the WRF-Chem model. In addition, the HONO formation parameterization needs to be improved in the model and sufficient measurements of the species associated with HONO are needed so that such a parameterization can be evaluated.

Acknowledgements

We thank Dr. Jianjun Li and Dr. Can Wu for providing the information of the IGAC instrument. This work was supported by the National Key R&D Plan (Quantitative Relationship and Regulation Principle between Regional Oxidation Capacity of Atmosphere and Air Quality (2017YFC0210000)) and National Natural Science Foundation of China (no. 41703127, 41430424, 41661144020). We also thank the editor and three anonymous reviewers for their comments which are very helpful for improving the paper.

Appendix A. Supplementary data

Supplementary data to this article can be found online at https://doi.org/10.1016/j.envpol.2018.09.069.

References

An, J., Li, Y., Chen, Y., Li, J., Qu, Y., Tang, Y., 2012. Enhancements of major aerosol components due to additional HONO sources in the North China Plain and implications for visibility and haze. Adv. Atmos. Sci. 30, 57–66. https://doi.org/10.1007/s00376-012-2016-9.

Arens, F., Gutzwiller, L., Baltensperger, U., Gäggeler, H.W., Ammann, M., 2001. Heterogeneous reaction of NO2on diesel soot particles. Environ. Sci. Technol. 35, 2191–2199. https://doi.org/10.1021/es000207s.

Aumont, B., Chervier, F., Laval, S., 2003. Contribution of HONO sources to the NOx/HOx/O3 chemistry in the polluted boundary layer. Atmos. Environ. 37, 487–498. https://doi.org/10.1016/s1352-2310(02)00920-2.

Bei, N., Li, G., Huang, R.-J., Cao, J., Meng, N., Feng, T., Liu, S., Zhang, T., Zhang, Q., Molina, L.T., 2016a. Typical synoptic situations and their impacts on the wintertime air pollution in the Guanzhong basin, China. Atmos. Chem. Phys. 16, 7373–7387. https://doi.org/10.5194/acp-16-7373-2016.

Bei, N., Li, G., Molina, L.T., 2012. Uncertainties in SOA simulations due to meteorological uncertainties in Mexico City during MILAGRO-2006 field campaign. Atmos. Chem. Phys. 12, 11295–11308. https://doi.org/10.5194/acp-12-11295-2012.

Bei, N., Wu, J., Elser, M., Feng, T., Cao, J., Haddad, El I., Li, X., Huang, R., Li, Z., Long, X., Xing, L., Zhao, S., Tie, X., Prévôt, A.S.H., Li, G., 2017. Impacts of meteorological uncertainties on the haze formation in Beijing–Tianjin–Hebei (BTH) during wintertime: a case study. Atmos. Chem. Phys. 17, 14579–14591. https://doi.org/10.5194/acp-17-14579-2017.

Bei, N., Xiao, B., Meng, N., Feng, T., 2016b. Critical role of meteorological conditions in a persistent haze episode in the Guanzhong basin, China. Sci. Total Environ. 550, 273–284. https://doi.org/10.1016/j.scitotenv.2015.12.159.

Bian, H., Chin, M., Hauglustaine, D.A., Schulz, M., Myhre, G., Bauer, S.E., Lund, M.T., Karydis, V.A., Kucsera, T.L., Pan, X., Pozzer, A., Skeie, R.B., Steenrod, S.D., Sudo, K., Tsigaridis, K., Tsimpidi, A.P., Tsyro, S.G., 2017. Investigation of global particulate nitrate from the AeroCom phase III experiment. Atmos. Chem. Phys. 17, 12911–12940. https://doi.org/10.5194/acp-17-12911-2017.

Binkowski, F.S., Roselle, S.J., 2003. Models-3 community multiscale air quality (CMAQ) model aerosol component 1. Model description. J. Geophys. Res. 108, 4183. https://doi.org/10.1029/2001JD001409.

Cao, J., Shen, Z.X., Chow, J.C., Watson, J.G., Lee, S.C., Tie, X.X., Ho, K.F., Wang, G.H., Han, Y.M., 2012a. Winter and summer PM2.5 chemical compositions in fourteen Chinese cities. J. Air Waste Manag. 62, 1214–1226. https://doi.org/10.1080/10962247.2012.701193.

Cao, J., Wang, Q.Y., Chow, J.C., Watson, J.G., Tie, X.X., Shen, Z.X., Wang, P., An, Z.S., 2012b. Impacts of aerosol compositions on visibility impairment in Xi'an, China. Atmos. Environ. 59, 559–566. https://doi.org/10.1016/j.atmosenv.2012.05.036.

Cao, J., Xu, H., Xu, Q., Chen, B., Kan, H., 2012c. Fine particulate matter constituents and cardiopulmonary mortality in a heavily polluted Chinese city. Environ. Health Perspect. 120, 373–378. https://doi.org/10.1289/ehp.1103671.

Cao, J.J., Wu, F., Chow, J.C., Lee, S.C., Li, Y., 2005. Characterization and source apportionment of atmospheric organic and elemental carbon during fall and winter of 2003 in Xi'an, China. Atmos. Chem. Phys. 5, 3127–3137. https://doi.org/10.5194/acp-5-3127-2005.

Chen, F., Dudhia, J., 2001. Coupling an advanced land surface-hydrology model with the Penn State-NCAR MM5 modeling system. Part II: preliminary model validation. Mon. Weather Rev. 129, 569–585. https://doi.org/10.1175/1520-0493(2001)129<0569:caalsh>2.0.co;2.

Cheng, Y., Zheng, G., Wei, C., Mu, Q., Zheng, B., Wang, Z., Gao, M., Zhang, Q., He, K., Carmichael, G., Po schl, U., Su, H., 2016. Reactive nitrogen chemistry in aerosol water as a source of sulfate during haze events in China. Sci. Adv. 2 https://doi.org/10.1126/sciadv.1601530 e1601530–e1601530.

Chou, M.-D., Suarez, M.J., 1999. A Solar Radiation Parameterization for Atmospheric Studies (No. NASA/TM-1999- 10460), NASA Technique Report.

Chou, M.-D., Suarez, M.J., Liang, X.-Z., Yan, M.M.H., 2001. A Thermal Infrared Radiation Parameterization for Atmospheric Studies (No. NASA/TM-2001-104606), NASA Technique Report.

Donahue, N.M., Robinson, A.L., Stanier, C.O., Pandis, S.N., 2006. Coupled partitioning, dilution, and chemical aging of semivolatile organics. Environ. Sci. Technol. 40, 2635–2643. https://doi.org/10.1021/es052297c.

Fairlie, T.D., Jacob, D.J., Dibb, J.E., Alexander, B., Avery, M.A., van Donkelaar, A., Zhang, L., 2010. Impact of mineral dust on nitrate, sulfate, and ozone in transpacific Asian pollution plumes. Atmos. Chem. Phys. 10, 3999–4012. https://doi.org/10.5194/acp-10-3999-2010.

Fast, J.D., Gustafson Jr., W.I., Easter, R.C., Zaveri, R.A., Barnard, J.C., Chapman, E.G., Grell, G.A., Peckham, S.E., 2006. Evolution of ozone, particulates, and aerosol direct radiative forcing in the vicinity of Houston using a fully coupled meteorology-chemistry-aerosol model. J. Geophys. Res. 111 https://doi.org/10.1029/2005JD006721, 2981–29.

Feng, T., Bei, N., Huang, R.-J., Cao, J., Zhang, Q., Zhou, W., Tie, X., Liu, S., Zhang, T., Su, X., Lei, W., Molina, L.T., Li, G., 2016a. Summertime ozone formation in Xi'an and surrounding areas, China. Atmos. Chem. Phys. 16, 4323–4342. https://doi.org/10.5194/acp-16-4323-2016.

Feng, T., Li, G., Cao, J., Bei, N., Shen, Z., Zhou, W., Liu, S., Zhang, T., Wang, Y., Huang, R.-J., Tie, X., Molina, L.T., 2016b. Simulations of organic aerosol concentrations during springtime in the Guanzhong Basin, China. Atmos. Chem. Phys. 16, 10045–10061. https://doi.org/10.5194/acp-16-10045-2016.

Ginoux, P., Chin, M., Tegen, I., Prospero, J.M., Holben, B., Dubovik, O., Lin, S.-J., 2001. Sources and distributions of dust aerosols simulated with the GOCART model. J. Geophys. Res. 106, 20255–20273. https://doi.org/10.1029/2000JD000053.

Grell, G.A., Peckham, S.E., Schmitz, R., McKeen, S.A., Frost, G., Skamarock, W.C., Eder, B., 2005. Fully coupled "online" chemistry within the WRF model. Atmos. Environ. 39, 6957–6975. https://doi.org/10.1016/j.atmosenv.2005.04.027.

Guenther, A., Karl, T., Harley, P., Wiedinmyer, C., Palmer, P.I., Geron, C., 2006. Estimates of global terrestrial isoprene emissions using MEGAN (model of emissions of gases and aerosols from nature). Atmos. Chem. Phys. 6, 3181–3210. https://doi.org/10.5194/acp-6-3181-2006.

Guo, H., Liu, J., Froyd, K.D., Roberts, J.M., Veres, P.R., Hayes, P.L., Jimenez, J.L., Nenes, A., Weber, R.J., 2017. Fine particle pH and gas–particle phase partitioning of inorganic species in Pasadena, California, during the 2010 CalNex campaign. Atmos. Chem. Phys. 17, 5703–5719. https://doi.org/10.5194/acp-17-5703-2017.

Guo, H., Sullivan, A.P., Campuzano-Jost, P., Schroder, J.C., Lopez-Hilfiker, F.D., Dibb, J.E., Jimenez, J.L., Thornton, J.A., Brown, S.S., Nenes, A., Weber, R.J., 2016. Fine particle pH and the partitioning of nitric acid during winter in the northeastern United States. J. Geophys. Res. 121 https://doi.org/10.1002/2016JD025311, 10,355–10,376.

Guo, H., Xu, L., Bougiatioti, A., Cerully, K.M., Capps, S.L., Hite Jr., J.R., Carlton, A.G., Lee, S.H., Bergin, M.H., Ng, N.L., Nenes, A., Weber, R.J., 2015. Fine-particle water and pH in the southeastern United States. Atmos. Chem. Phys. 15, 5211–5228. https://doi.org/10.5194/acp-15-5211-2015.

Gutzwiller, L., Arens, F., Baltensperger, U., Gäggeler, H.W., Ammann, M., 2002. Significance of semivolatile diesel exhaust organics for secondary HONO formation. Environ. Sci. Technol. 36, 677–682. https://doi.org/10.1021/es015673b.

Hong, S.Y., Lim, J., 2006. The WRF single-moment 6-class microphysics scheme (WSM6). Asia-Pac. J. Atmos. Sci. 42, 129–151.

Horowitz, L.W., Walters, S., Mauzerall, D.L., Emmons, L.K., Rasch, P.J., Granier, C., Tie, X., Lamarque, J.-F., Schultz, M.G., Tyndall, G.S., Orlando, J.J., Brasseur, G.P., 2003. A global simulation of tropospheric ozone and related tracers: description and evaluation of MOZART, version 2. J. Geophys. Res. 108, 4784. https://doi.org/10.1029/2002jd002853.

Huang, R.-J., Yang, L., Cao, J., Wang, Q., Tie, X., Ho, K.F., Shen, Z., Zhang, R., Li, G., Zhu, C., Zhang, N., Dai, W., Zhou, J., Liu, S., Chen, Y., Chen, J., O'Dowd, C.D., 2017. Concentration and sources of atmospheric nitrous acid (HONO) at an urban site in Western China. Sci. Total Environ. 593–594, 165–172. https://doi.org/10.1016/j.scitotenv.2017.02.166.

Huang, R.-J., Zhang, Y., Bozzetti, C., Ho, K.F., Cao, J., Han, Y., Daellenbach, K.R., Slowik, J.G., Platt, S.M., Canonaco, F., Zotter, P., Wolf, R., Pieber, S.M., Bruns, E.A., Crippa, M., Ciarelli, G., Piazzalunga, A., Schwikowski, M., Abbaszade, G., Schnelle-Kreis, J., Zimmermann, R., An, Z., Szidat, S., Baltensperger, U., Haddad, El I., Prévôt, A.S.H., 2014. High secondary aerosol contribution to particulate pollution during haze events in China. Nature 514, 218–222. https://doi.org/10.1038/nature13774.

Itahashi, S., Uno, I., Osada, K., Kamiguchi, Y., Yamamoto, S., Tamura, K., Wang, Z., Kurosaki, Y., Kanaya, Y., 2017. Nitrate transboundary heavy pollution over East Asia in winter. Atmos. Chem. Phys. 17, 3823–3843. https://doi.org/10.5194/acp-17-3823-2017.

Janjić, Z.I., 2002. Nonsingular Implementation of the Mellor–Yamada Level 2.5 Scheme in the NCEP Meso Model. NCEP office note, No. 437, pp. 1–61.

Karydis, V.A., Tsimpidi, A.P., Lei, W., Molina, L.T., Pandis, S.N., 2011. Formation of semivolatile inorganic aerosols in the Mexico City Metropolitan Area during the MILAGRO campaign. Atmos. Chem. Phys. 11, 13305–13323. https://doi.org/10.5194/acp-11-13305-2011.

Karydis, V.A., Tsimpidi, A.P., Pozzer, A., Astitha, M., Lelieveld, J., 2016. Effects of mineral dust on global atmospheric nitrate concentrations. Atmos. Chem. Phys. 16, 1491–1509. https://doi.org/10.5194/acp-16-1491-2016.

Lei, H., Wuebbles, D.J., 2013. Chemical competition in nitrate and sulfate formations and its effect on air quality. Atmos. Environ. 80, 472–477. https://doi.org/10.1016/j.atmosenv.2013.08.036.

Li, G., Bei, N., Cao, J., Huang, R., Wu, J., Feng, T., Wang, Y., Liu, S., Zhang, Q., Tie, X., Molina, L.T., 2017. A possible pathway for rapid growth of sulfate during haze days in China. Atmos. Chem. Phys. 17, 3301–3316. https://doi.org/10.5194/acp-17-3301-2017.

Li, G., Bei, N., Tie, X., Molina, L.T., 2011a. Aerosol effects on the photochemistry in Mexico City during MCMA-2006/MILAGRO campaign. Atmos. Chem. Phys. 11, 5169–5182. https://doi.org/10.5194/acp-11-5169-2011.

Li, G., Bei, N., Tie, X., Molina, L.T., 2011b. Aerosol effects on the photochemistry in Mexico City during MCMA-2006/MILAGRO campaign. Atmos. Chem. Phys. 11, 5169–5182. https://doi.org/10.5194/acp-11-5169-2011.

Li, G., Lei, W., Zavala, M., Volkamer, R., Dusanter, S., Stevens, P., Molina, L.T., 2010. Impacts of HONO sources on the photochemistry in Mexico city during the MCMA-2006/MILAGO campaign. Atmos. Chem. Phys. 10, 6551–6567. https://doi.org/10.5194/acp-10-6551-2010.

Li, G., Zavala, M., Lei, W., Tsimpidi, A.P., Karydis, V.A., Pandis, S.N., Canagaratna, M.R., Molina, L.T., 2011c. Simulations of organic aerosol concentrations in Mexico City using the WRF-CHEM model during the MCMA-2006/MILAGRO campaign. Atmos. Chem. Phys. 11, 3789–3809. https://doi.org/10.5194/acp-11-3789-2011.

Li, G., Zhang, R., Fan, J., Tie, X., 2005. Impacts of black carbon aerosol on photolysis and ozone. J. Geophys. Res. 110, D23206. https://doi.org/10.1029/2005JD005898.

Li, L., Hoffmann, M.R., Colussi, A.J., 2018. Role of nitrogen dioxide in the production of sulfate during Chinese haze-aerosol episodes. Environ. Sci. Technol. 52, 2686–2693. https://doi.org/10.1021/acs.est.7b05222.

Li, Y., An, J., Min, M., Zhang, W., Wang, F., Xie, P., 2011. Impacts of HONO sources on the air quality in Beijing, Tianjin and Hebei province of China. Atmos. Environ.

45, 4735–4744. https://doi.org/10.1016/j.atmosenv.2011.04.086.
Liu, M., Song, Y., Zhou, T., Xu, Z., Yan, C., Zheng, M., Wu, Z., Hu, M., Wu, Y., Zhu, T., 2017. Fine particle pH during severe haze episodes in northern China. Geophys. Res. Lett. 44, 5213–5221. https://doi.org/10.1002/2017GL073210.
Morgan, W.T., Allan, J.D., Bower, K.N., Esselborn, M., Harris, B., Henzing, J.S., Highwood, E.J., Kiendler-Scharr, A., McMeeking, G.R., Mensah, A.A., Northway, M.J., Osborne, S., Williams, P.I., Krejci, R., Coe, H., 2010. Enhancement of the aerosol direct radiative effect by semi-volatile aerosol components: airborne measurements in North-Western Europe. Atmos. Chem. Phys. 10, 8151–8171. https://doi.org/10.5194/acp-10-8151-2010.
Morino, Y., Kondo, Y., Takegawa, N., Miyazaki, Y., Kita, K., Komazaki, Y., Fukuda, M., Miyakawa, T., Moteki, N., Worsnop, D.R., 2006. Partitioning of HNO3 and particulate nitrate over Tokyo: effect of vertical mixing. J. Geophys. Res. 111, D15215–D15219. https://doi.org/10.1029/2005JD006887.
Nenes, A., Pandis, S.N., Pilinis, C., 1998. ISORROPIA: a New thermodynamic equilibrium model for multiphase multicomponent inorganic aerosols. Aquat. Geochem. 4, 123–152. https://doi.org/10.1023/A:1009604003981.
Poulain, L., Spindler, G., Birmili, W., Plass-Dülmer, C., Wiedensohler, A., Herrmann, H., 2011. Seasonal and diurnal variations of particulate nitrate and organic matter at the IfT research station Melpitz. Atmos. Chem. Phys. 11, 12579–12599. https://doi.org/10.5194/acp-11-12579-2011.
Pozzer, A., Tsimpidi, A.P., Karydis, V.A., de Meij, A., Lelieveld, J., 2017. Impact of agricultural emission reductions on fine-particulate matter and public health. Atmos. Chem. Phys. 17, 12813–12826. https://doi.org/10.5194/acp-17-12813-2017.
Robinson, A.L., Donahue, N.M., Shrivastava, M.K., Weitkamp, E.A., Sage, A.M., Grieshop, A.P., Lane, T.E., Pierce, J.R., Pandis, S.N., 2007. Rethinking organic aerosols: semivolatile emissions and photochemical aging. Science 315, 1259–1262. https://doi.org/10.1126/science.1133061.
Seinfeld, J.H., Pandis, S.N., 2006. Atmospheric Chemistry and Physics - from Air Pollution to Climate Change, second ed. John Wiley & Sons, New Jersey.
Shen, Z., Arimoto, R., Cao, J., Zhang, R., Li, X., 2008. Seasonal variations and evidence for the effectiveness of pollution controls on water-soluble inorganic species in total suspended particulates and fine particulate matter from Xi'an, China. J. Air Waste Manag. 58, 1560–1570. https://doi.org/10.3155/1047-3289.58.12.1560.
Shen, Z., Cao, J., Arimoto, R., Han, Z., Zhang, R., Han, Y., Liu, S., Okuda, T., Nakao, S., Tanaka, S., 2009. Ionic composition of TSP and PM2.5 during dust storms and air pollution episodes at Xi'an, China. Atmos. Environ. 43, 2911–2918. https://doi.org/10.1016/j.atmosenv.2009.03.005.
Shrivastava, M.K., Lane, T.E., Donahue, N.M., Pandis, S.N., Robinson, A.L., 2008. Effects of gas particle partitioning and aging of primary emissions on urban and regional organic aerosol concentrations. J. Geophys. Res. 113, D18301–D18316. https://doi.org/10.1029/2007JD009735.
Tang, G., Zhang, J., Zhu, X., Song, T., Münkel, C., Hu, B., Schäfer, K., Liu, Z., Zhang, J., Wang, L., Xin, J., Suppan, P., Wang, Y., 2016. Mixing layer height and its implications for air pollution over Beijing, China. Atmos. Chem. Phys. 16, 2459–2475. https://doi.org/10.5194/acp-16-2459-2016.
Tian, M., Wang, H., Chen, Y., Zhang, L., Shi, G., Liu, Y., Yu, J., Zhai, C., Wang, J., Yang, F., 2017. Highly time-resolved characterization of water-soluble inorganic ions in PM2.5 in a humid and acidic mega city in Sichuan Basin, China. Sci. Total Environ. 580, 224–234. https://doi.org/10.1016/j.scitotenv.2016.12.048.
Tie, X., Madronich, S., Walters, S., Zhang, R., Rasch, P., Collins, W., 2003. Effect of clouds on photolysis and oxidants in the troposphere. J. Geophys. Res. 108, 4642. https://doi.org/10.1029/2003JD003659.
Trump, E.R., Fountoukis, C., Donahue, N.M., Pandis, S.N., 2015. Improvement of simulation of fine inorganic PM levels through better descriptions of coarse particle chemistry. Atmos. Environ. 102, 274–281. https://doi.org/10.1016/j.atmosenv.2014.11.059.
Tsimpidi, A.P., Karydis, V.A., Zavala, M., 2010. Evaluation of the volatility basis-set approach for the simulation of organic aerosol formation in the Mexico City metropolitan area. Atmos. Chem. Phys. 10, 525–546. https://doi.org/10.5194/acp-10-525-2010.
Volkamer, R., San Martini, F., Molina, L.T., Salcedo, D., Jimenez, J.L., Molina, M.J., 2007. A missing sink for gas-phase glyoxal in Mexico City: formation of secondary organic aerosol. Geophys. Res. Lett. 34, L19807. https://doi.org/10.1029/2007GL030752.
Wang, G., Zhang, R., Gomez, M.E., Yang, L., Levy Zamora, M., Hu, M., Lin, Y., Peng, J., Guo, S., Meng, J., Li, J., Cheng, C., Hu, T., Ren, Y., Wang, Y., Gao, J., Cao, J., An, Z., Zhou, W., Li, G., Wang, J., Tian, P., Marrero-Ortiz, W., Secrest, J., Du, Z., Zheng, J., Shang, D., Zeng, L., Shao, M., Wang, W., Huang, Y., Wang, Y., Zhu, Y., Li, Y., Hu, J., Pan, B., Cai, L., Cheng, Y., Ji, Y., Zhang, F., Rosenfeld, D., Liss, P.S., Duce, R.A., Kolb, C.E., Molina, M.J., 2016. Persistent sulfate formation from London Fog to Chinese haze. Proc. Natl. Acad. Sci. U. S. A. https://doi.org/10.1073/pnas.1616540113, 201616540–18.
Wang, Y., Wang, M., Zhang, R., Ghan, S.J., Lin, Y., Hu, J., Pan, B., Levy, M., Jiang, J.H., Molina, M.J., 2014a. Assessing the effects of anthropogenic aerosols on Pacific storm track using a multiscale global climate model. Proc. Natl. Acad. Sci. U.S.A. 111, 6894–6899. https://doi.org/10.1073/pnas.1403364111.
Wang, Y., Zhang, R., Saravanan, R., 2014b. Asian pollution climatically modulates mid-latitude cyclones following hierarchical modelling and observational analysis. Nat. Commun. 5, 3098. https://doi.org/10.1038/ncomms4098.
Wesely, M.L., 1989. Parameterization of surface resistances to gaseous dry deposition in regional-scale numerical models. Atmos. Environ. 23, 1293–1304. https://doi.org/10.1016/0004-6981(89)90153-4 (1967).
Wu, J., Bei, N., Li, X., Cao, J., Feng, T., Wang, Y., Tie, X., Li, G., 2018. Widespread air pollutants of the North China Plain during the Asian summer monsoon season: a case study. Atmos. Chem. Phys. 18, 8491–8504. https://doi.org/10.5194/acp-18-8491-2018.
Wu, J., Li, G., Cao, J., Bei, N., Wang, Y., Feng, T., Huang, R., Liu, S., Zhang, Q., Tie, X., 2017. Contributions of trans-boundary transport to summertime air quality in Beijing, China. Atmos. Chem. Phys. 17, 2035–2051. https://doi.org/10.5194/acp-17-2035-2017.
Young, L.-H., Li, C.-H., Lin, M.-Y., Hwang, B.-F., Hsu, H.-T., Chen, Y.-C., Jung, C.-R., Chen, K.-C., Cheng, D.-H., Wang, V.-S., Chiang, H.-C., Tsai, P.-J., 2016. Field performance of a semi-continuous monitor for ambient PM2.5 water-soluble inorganic ions and gases at a suburban site. Atmos. Environ. 144, 376–388. https://doi.org/10.1016/j.atmosenv.2016.08.062.
Zhang, Q., Streets, D.G., Carmichael, G.R., 2009. Asian emissions in 2006 for the NASA INTEX-B mission. Atmos. Chem. Phys. 9, 5131–5153. https://doi.org/10.5194/acp-9-5131-2009.
Zhang, R., Li, G., Fan, J., Wu, D.L., Molina, M.J., 2007. Intensification of Pacific storm track linked to Asian pollution. Proc. Natl. Acad. Sci. U.S.A. 104, 5295–5299. https://doi.org/10.1073/pnas.0700618104.
Zhao, J., Levitt, N.P., Zhang, R., Chen, J., 2006. Heterogeneous reactions of methylglyoxal in acidic media: implications for secondary organic aerosol formation. Environ. Sci. Technol. 40, 7682–7687. https://doi.org/10.1021/es060610k.
Zhao, S., Tie, X., Cao, J., Zhang, Q., 2015. Impacts of mountains on black carbon aerosol under different synoptic meteorology conditions in the Guanzhong region, China. Atmos. Res. 164–165, 286–296. https://doi.org/10.1016/j.atmosres.2015.05.016.
Zheng, G.J., Duan, F.K., Su, H., Ma, Y.L., Cheng, Y., Zheng, B., Zhang, Q., Huang, T., Kimoto, T., Chang, D., Pöschl, U., Cheng, Y.F., He, K.B., 2015. Exploring the severe winter haze in Beijing: the impact of synoptic weather, regional transport and heterogeneous reactions. Atmos. Chem. Phys. 15, 2969–2983. https://doi.org/10.5194/acp-15-2969-2015.
Zhou, X., Gao, H., He, Y., Huang, G., Bertman, S.B., Civerolo, K., Schwab, J., 2003. Nitric acid photolysis on surfaces in low-NOxenvironments: significant atmospheric implications. Geophys. Res. Lett. 30, 1–12. https://doi.org/10.1029/2003gl018620.
Zhou, X., Zhang, N., TerAvest, M., Tang, D., Hou, J., Bertman, S., Alaghmand, M., Shepson, P.B., Carroll, M.A., Griffith, S., Dusanter, S., Stevens, P.S., 2011. Nitric acid photolysis on forest canopy surface as a source for tropospheric nitrous acid. Nat. Geosci. 4, 440–443. https://doi.org/10.1038/ngeo1164.